

Semigrand-canonical ensemble simulations of the phase diagrams of alloys

F M Marquez¹, C Cienfuegos², B K Pongsai³, M Yu Lavrentiev^{3,5},
N L Allan³, J A Purton⁴ and G D Barrera¹

¹ Departamento de Química, Universidad Nacional de la Patagonia SJB, Ciudad Universitaria, (9005) Comodoro Rivadavia, Argentina

² Departamento de Química Inorgánica, Analítica y Química Física, Facultad de Ciencias Exactas y Naturales, Universidad de Buenos Aires, Pab. 2, Ciudad Universitaria, (1428) Buenos Aires, Argentina

³ School of Chemistry, University of Bristol, Cantock's Close, Bristol BS8 1TS, UK

⁴ CLRC, Daresbury Laboratory, Warrington, Cheshire WA4 4AD, UK

Received 15 July 2002, in final form 20 November 2002

Published 10 January 2003

Online at stacks.iop.org/MSMSE/11/115

Abstract

We show how Monte Carlo simulations with the explicit interchange of atoms and the use of the semigrand-canonical ensemble, can be used to calculate phase diagrams for alloys. We illustrate our approach with the system Pd/Rh using the embedded atom method with potential parameters derived from *ab initio* density functional calculations. Our techniques take full account of local structural distortion, clustering and thermal effects.

1. Introduction

Solid solutions and phase stability present considerable challenges for theory. Energy differences between different phases can be small and subtle ordering effects can often be crucial in determining phase stability and thermodynamic and chemical properties. Disorder has largely been investigated theoretically via point defect calculations (the dilute limit), or via 'supercells', introducing a superlattice of defects which extends throughout the macroscopic crystal. The periodicity is then that of the particular superlattice chosen and convergence towards properties of an isolated defect occurs as the superlattice spacing is increased. These two methods are not readily extended to solid solutions, liquid phases or disordered systems with a *finite* impurity or defect content far from the dilute limit. The *ab initio* calculation of solid-state alloy phase diagrams has been largely based on generalized lattice-model Hamiltonians (see, e.g. [1]) and the cluster variation method.

We are currently developing a series of new codes and methods, for metals [2] and for ceramics [3, 4], to address such problems. A key feature of all of these is the need to sample many different arrangements of atoms, allowing for the exchange of atoms located at

⁵ On leave from the Institute of Inorganic Chemistry, 630090 Novosibirsk, Russia.

crystallographically inequivalent positions. Any method must also take into account the local environment of each ion and the local structural movements (relaxation), which accompany any exchange of atoms and reduce considerably the energy associated with any such interchange. Local effects due to clustering should not be averaged out. Methods should be readily extendible to incorporate the effects of high pressure or thermal (vibrational) effects.

Our approach is illustrated using the system Pd/Rh, which has been shown experimentally to have a miscibility gap, with a critical temperature of about 1200 K at $x(\text{Rh}) \approx 0.5$ [5–7]. In a recent study Jacob *et al* [7] have reported positive excess enthalpies, free energies and entropies of mixing at 1273 K. Metastable disordered Pd–Rh alloys are stable from ambient to relatively high temperatures [6].

We work within the framework of the embedded atom method (EAM) [8–10]. A novel feature of our use of this model is that interatomic potentials are obtained by fitting to energy hypersurfaces obtained from *ab initio* density functional calculations (cf [11]). Such a procedure is likely to be especially valuable for problems involving disordered systems and mixtures where, due to local structural relaxation, interatomic distances may be substantially different from those adopted in pure end members.

2. Theoretical methods

2.1. The embedded atom method

In the EAM [8–10], the static energy of the crystal may be written as

$$\Phi_{\text{stat}} = \sum_i F_i(\rho_i) + \frac{1}{2} \sum_i \sum_j' \phi_{ij}(r_{ij}) \quad (1)$$

Primes on summations in this and subsequent equations indicate that terms with $r_{ij} = 0$ are excluded. $F_i(\rho_i)$ is negative and represents the energy of ‘embedding’ atom i in the electronic density ρ_i created by all other atoms in the crystal, and ϕ_{ij} is the core–core repulsion between atoms i and j , assumed to depend only on the type of the atoms i and j and the distance between them. The electron density ρ_i is assumed to be the sum of the electronic densities of all other atoms at the nucleus of atom i :

$$\rho_i = \sum_j' f_j(r_{ij}) \quad (2)$$

where the electron density created by atom j at a distance r_{ij} , $f_j(r_{ij})$, is assumed to be isotropic about atom j . As implemented here EAM includes certain many-body contributions to the crystal energy while the computational effort is reduced by not including angular contributions explicitly. The parameters within the model are obtained using an *ab initio* potential energy hypersurfaces as described below.

2.2. Monte Carlo simulations

We use Monte Carlo exchange (MCX) simulations [12, 13], in the NPT ensemble. In any step, a random choice is made whether to attempt a random exchange between two atoms, a random displacement of an ion, or a random change in the volume of the simulation box. To determine whether any change is accepted or rejected, the usual Metropolis algorithm [14, 15] is applied. The maximum changes in the atomic displacements and the lattice parameters are governed by the variables r_{max} and v_{max} , respectively. The magnitudes of these parameters are adjusted automatically during the equilibration part of the simulation to maintain an acceptance/rejection ratio of approximately 0.3. Most of the Monte Carlo calculations reported here used a cubic

box containing 256 atoms ($4 \times 4 \times 4$ primitive cubic unit cells) and 5×10^7 data collection steps, following initial equilibration of 1×10^7 steps. Runs with larger cells were carried out in order to check convergence.

3. Results

3.1. Potential parametrization

We choose a simple form for the potential. For the electronic densities, the f_j (equation (2)), exponential functions are used:

$$f_j(r_{ij}) = D_j \exp\left(\frac{-r_{ij}}{\xi_j}\right) \quad (3)$$

with different parameters D_j and ξ_j for each metal ($j = \text{Pd, Rh}$) and with a cut-off of 6 Å. The embedding energy (equation (1)) is given by

$$F_j(\rho_j) = -C_j \sqrt{\rho_j} \quad (4)$$

with different parameters C_j again for Pd and Rh. The repulsive potential in equation (1) is also given a simple form,

$$\phi_{ij}(r_{ij}) = A_{ij} \exp\left(\frac{-r_{ij}}{\sigma_{ij}}\right) \quad (5)$$

where A_{ij} and σ_{ij} are different for each type of interaction (Pd–Pd, Rh–Rh, Pd–Rh).

Thus, for each pure metal there are five parameters to be determined and the Pd–Rh repulsive interaction requires a further two. One simplification is to put $C_{\text{Rh}} = 1$ without loss of generality, since the energy of any configuration depends only on $C_{\text{Rh}} \sqrt{D_{\text{Rh}}}$.

We have obtained values for the remaining parameters by fitting to the results of *ab initio* full-potential linearized augmented plane wave (FP-LAPW) calculations, using the generalized gradient approximation (GGA) [16] as implemented in the WIEN97 code [17]. The LAPW method divides the unit cell into nonoverlapping atomic spheres and an interstitial region. The solutions to the Kohn–Sham equations [18] are expanded in a combined basis set of LAPWs—a linear combination of radial functions multiplied by spherical harmonics inside the atomic spheres, and plane waves in the interstitial region. The method is free of shape approximations to the charge density or the potential. The calculations were non-spin-polarized and the exchange-correlation contributions to the total energy were obtained within the GGA. For integration in reciprocal space 5000 k -points over the entire Brillouin zone were used. The muffin-tin radius for both Rh and Pd was set to 2.4 a.u. while the product of the muffin-tin radius, R_{MT} , and the maximum reciprocal space vector, k_{max} , was put equal to 10. The maximum l value for the waves inside the atomic spheres, l_{max} , and the largest G in the charge Fourier expansion, G_{max} , were set to 12 and 24, respectively. The convergence criteria for the SCF calculations was taken as 0.0001 in charge differences.

These first principles calculations were carried out for the following structures:

- (a) pure Rh and Pd, both in the face centred cubic structure, and for values of the lattice parameter a shown in figures 1(a) and (b);
- (b) Rh_3Pd as a simple cubic lattice with Rh atoms at $(0, \frac{1}{2}, \frac{1}{2})$, $(\frac{1}{2}, 0, \frac{1}{2})$, $(\frac{1}{2}, \frac{1}{2}, 0)$, Pd atoms at $(0, 0, 0)$, and for the range of lattice parameter a shown in figure 1(c);
- (c) RhPd_3 with the same structure as Rh_3Pd for the values of the lattice parameter a shown in figure 1(d);

- (d) RhPd as a tetragonal lattice with Rh atoms at $(0, 0, 0)$ and Pd atoms at $(\frac{1}{2}, \frac{1}{2}, \frac{1}{2})$. Each (approximate) parabola for the configurations of RhPd shown in figure 2(a) corresponds, from left to right, to values of c from 3.7 to 4.0 Å in steps of 0.1 Å. Within each parabola the configurations shown correspond to values of a from 2.6 to 3.2 Å in steps of 0.2 Å;
- (e) RhPd as a tetragonal lattice with Rh atoms at $(0, 0, 0)$ and $(\frac{1}{2}, \frac{1}{2}, \frac{1}{4})$, and Pd atoms at $(0, 0, \frac{1}{2})$ and $(\frac{1}{2}, \frac{1}{2}, \frac{3}{4})$. The configurations shown in figure 2(b) correspond to values of c from 7.4 to 7.8 Å in steps of 0.2 Å with values of a within each parabola from 2.6 to 3.2 Å, again in steps of 0.2 Å. This corresponds to a supercell of the type described above in (d) but with a pair of Rh and Pd atoms interchanged. It is introduced to allow the sampling of configurations with less symmetry than that in (d).

As seen from figures 1 and 2 the energy hypersurface resulting from the adjusted potential reproduces very well the *ab initio* results. All the potential parameters are collected together in table 1.

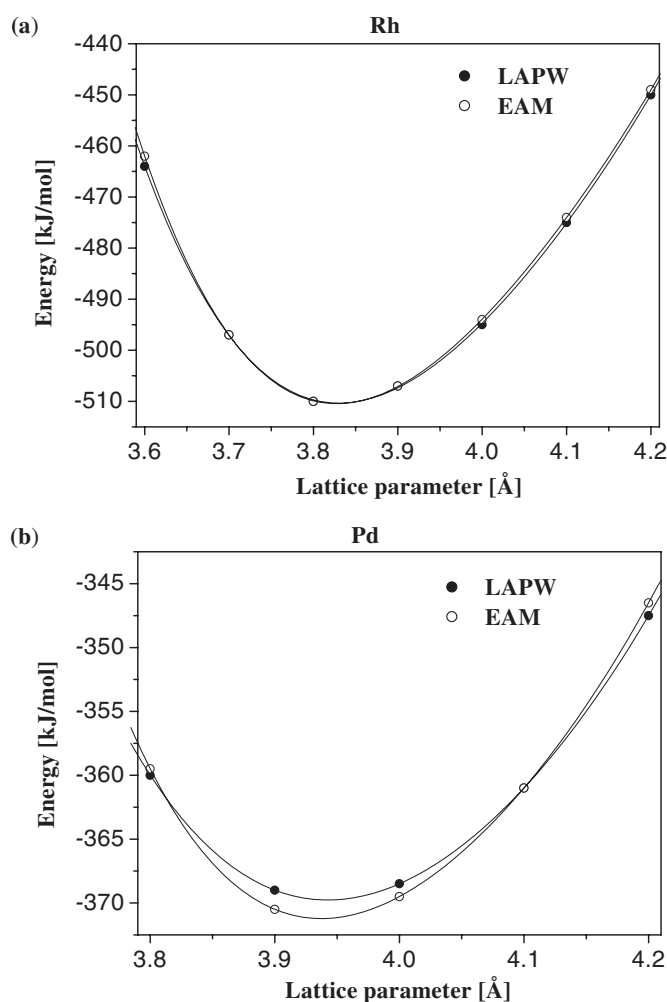


Figure 1. Energy vs lattice parameter for (a) Rh, (b) Pd, (c) Rh₃Pd and (d) RhPd₃ from the LAPW calculations and the resulting EAM potential.

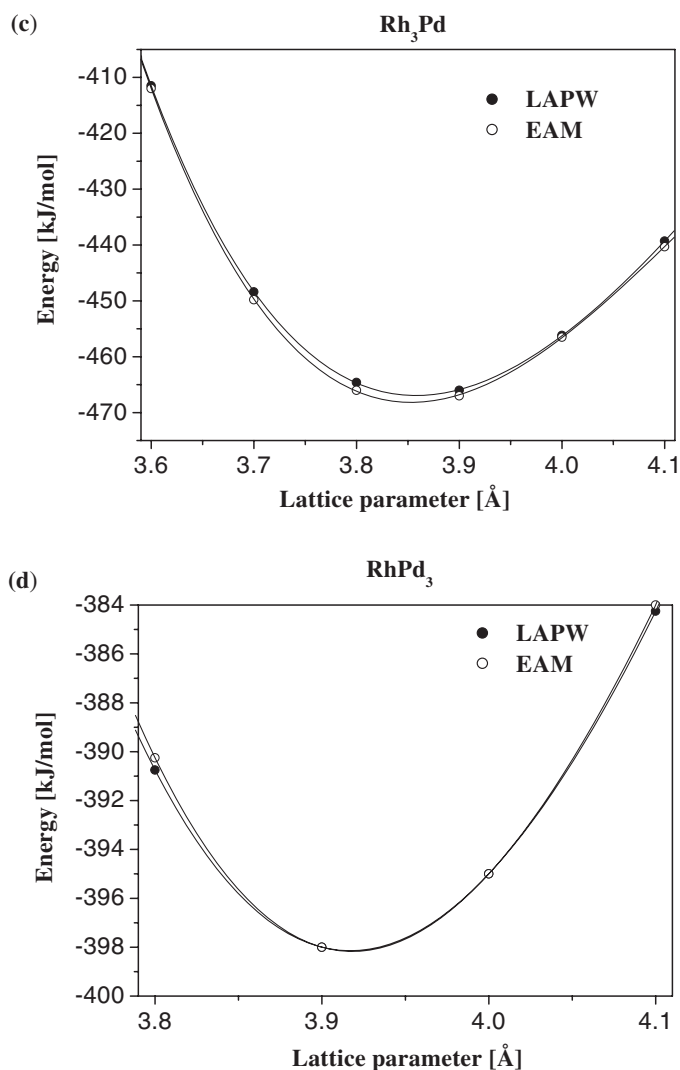


Figure 1. (Continued)

3.2. Thermodynamics of mixing

We consider first the enthalpies of mixing, calculated via MCX simulations. Figure 3 shows calculated values of ΔH_{mix} at 1273 K, together with experimental results from [6]. There is at least qualitative agreement, although the experimental results are somewhat larger than those obtained from the simulation, particularly for the 50/50 mixture. In this context it is important to note that ΔH_{mix} is predicted to vary markedly with temperature as illustrated in figure 4 for Pd_{0.5}Rh_{0.5}; there is a steady increase from 500 to 1400 K, over which range ΔH_{mix} almost doubles. This figure also illustrates the rapid convergence of ΔH_{mix} with simulation cell size for this system, justifying our choice of a simulation cell for most of the calculations comprising 256 atoms.

Calculation of the free energy is less straightforward. Absolute magnitudes of this quantity cannot be obtained readily from Monte Carlo calculations. However, the calculation of the

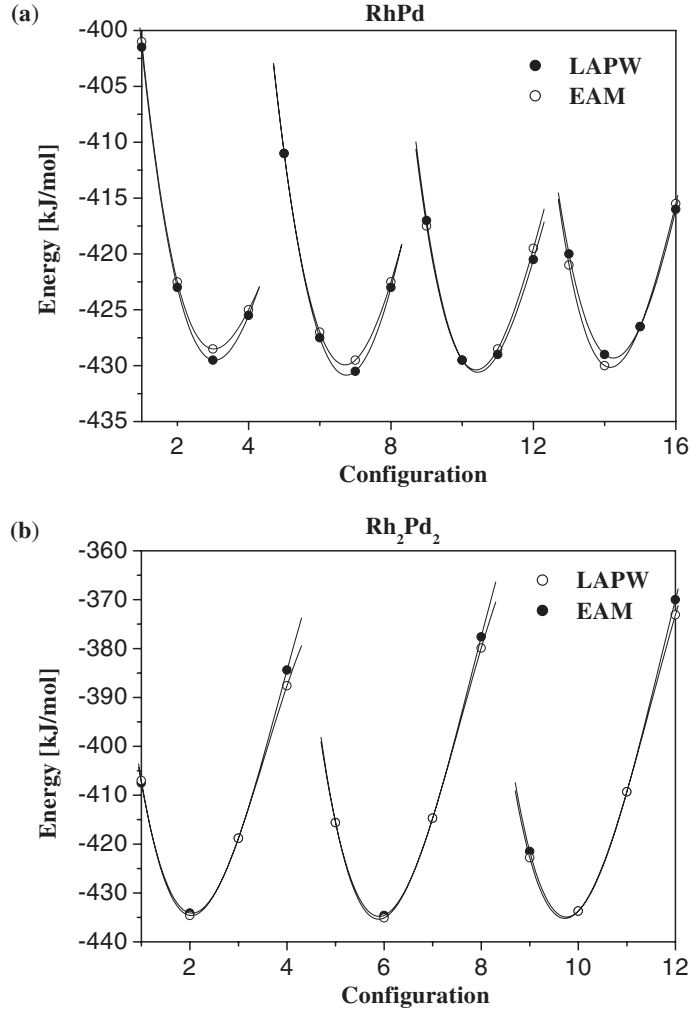


Figure 2. Energy for a range of configurations of (a) tetragonal RhPd and (b) the tetragonal cell with four atoms per unit cell (Rh₂Pd₂) described in the text, from LAPW calculations and the resulting EAM potential. For the atomic coordinates see points (d) and (e) in the list in the text for parts (a) and (b), respectively. Each configuration corresponds to different values of the lattice parameters a and c , as explained in the text.

Table 1. The potential parameters, obtained by fitting to *ab initio* energy hypersurfaces, used in this work.

i/j	A_{ij} (eV)	σ_{ij} (Å)	C_j (eV)	D_j	ζ_j (Å)
Rh	26 294.5	0.246 062	1.0	7119.18	0.373 618
Pd	129 054	0.208 140	0.757 357	1620.58	0.453 342
Rh-Pd	27 060.4	0.241 988	—	—	—

phase diagram requires *free energy differences* rather than absolute values, and here we have resorted to novel Monte Carlo techniques used for liquids. We use semigrand-canonical ensemble simulations [15, 19] to calculate the difference in chemical potential of Pd and Rh atoms. In this method one species, B, is converted into another, A, and the resulting potential

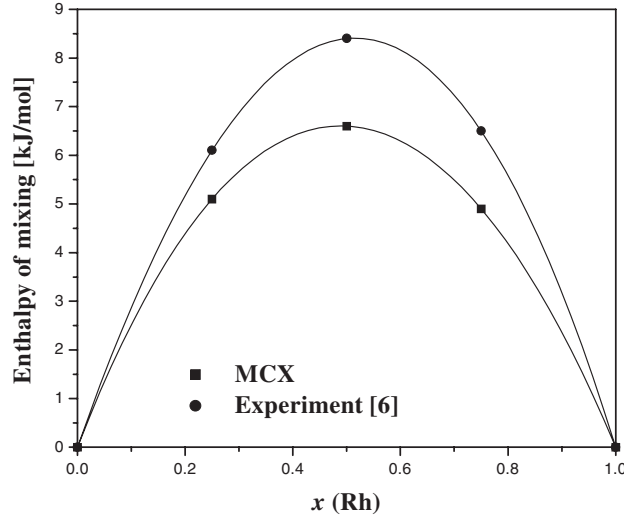


Figure 3. Enthalpies of mixing at 1273 K calculated using MCX (256-atom cell) compared with the experimental data of Jacob *et al* [6] at the same temperature.

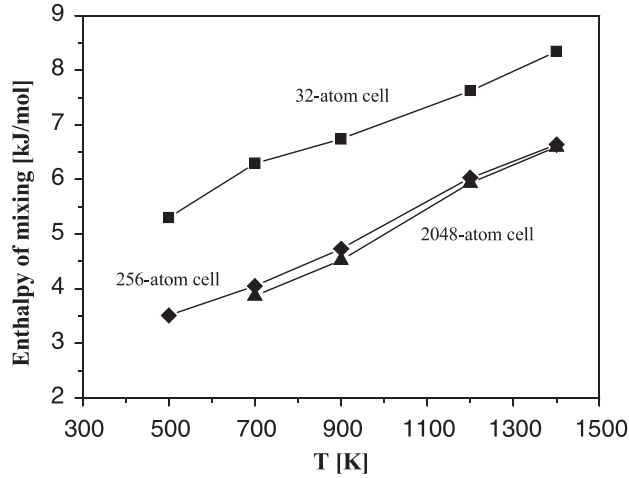


Figure 4. The temperature dependence of ΔH_{mix} (500–1400 K) calculated using the MCX method, with 32-, 256- and 2048-atom cells for $\text{Pd}_{0.5}\text{Rh}_{0.5}$.

energy change $\Delta U_{\text{B/A}}$ determined. This is related to the change in chemical potential $\Delta\mu_{\text{B/A}}$ by

$$\Delta\mu_{\text{B/A}} = -k_{\text{B}}T \ln \left\langle \frac{N_{\text{B}}}{N_{\text{A}} + 1} \exp \left(\frac{-\Delta U_{\text{B/A}}}{k_{\text{B}}T} \right) \right\rangle \quad (6)$$

Each fifth step (on average) we evaluate the energy associated with the conversion of a randomly chosen Rh atom to Pd, $\Delta U_{\text{Rh/Pd}}$, and as the simulation proceeds determine the average value of the exponential in equation (6). Note that the change of Rh into Pd is only considered but *not* actually performed—the configuration remains unchanged after evaluating $\Delta U_{\text{Rh/Pd}}$. The remainder of the simulation is as for the MCX approach described above. We have checked consistency in that, overall, identical results are obtained considering the reverse

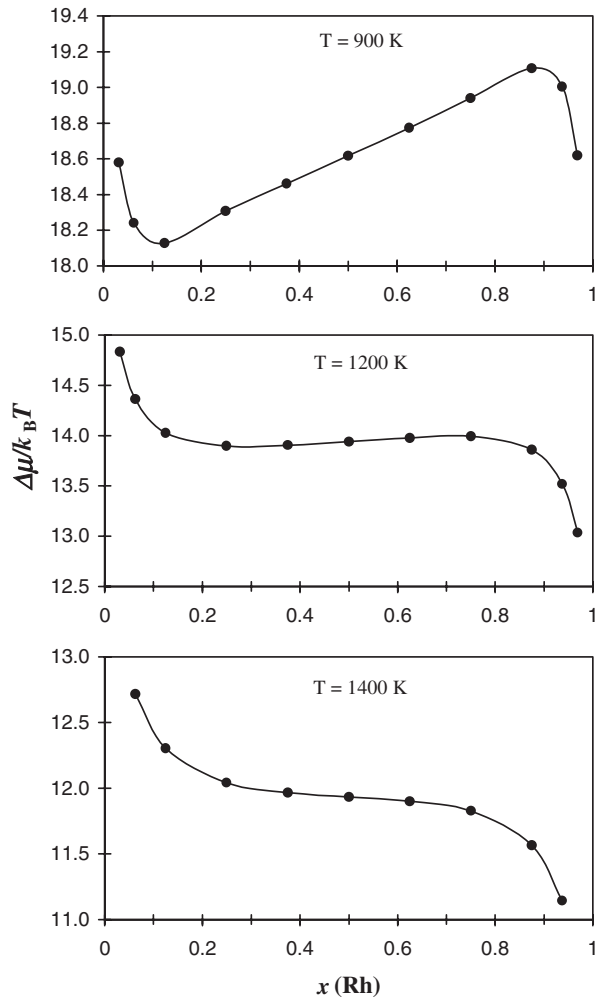


Figure 5. Variation of $\Delta\mu_{\text{Rh/Pd}}/k_{\text{B}}T$ ($=\mu_{\text{Pd}} - \mu_{\text{Rh}}$) vs $x(\text{Rh})$ at 900, 1200 and 1400 K.

transformation, i.e. of a randomly chosen Pd to a Rh atom. Note that our approach differs somewhat from the methods of Laradji *et al* [20] since the change of one atom into another is only noted but not performed in our simulations; our implementation of the semigrand-canonical ensemble is more in line with the treatment in [15].

We show the calculated variation of $\Delta\mu_{\text{Rh/Pd}}/k_{\text{B}}T$ with $x(\text{Rh})$ at three temperatures (at 900, 1200 and 1400 K), using a 256-atom cell for $\text{Pd}_{1-x}\text{Rh}_x$, in figure 5. The existence of a maximum and a minimum in a $\Delta\mu(x)$ curve indicates two minima in $\Delta G(x)$ vs x and thus a miscibility gap at that temperature. It is clear from the shapes of these curves that 900 K corresponds to a temperature below the consolute temperature, with the formation of one- and two-phase regions at different compositions. The observed consolute temperature, 1200 K [5, 7, 21], is just below the calculated consolute temperature, as indicated by the shape of the $\Delta\mu(x)$ curve in which the stationary points evident at 900 K have almost disappeared. At 1400 K they are not present and this is above the consolute temperature, indicating complete miscibility and the formation of a single phase at all compositions.

To calculate the phase diagram, the calculated values of $\Delta\mu(x_{\text{Rh}})$ are fitted to a cubic polynomial in x_{Rh} :

$$\frac{\Delta\mu}{k_{\text{B}}T} = \frac{\Delta\mu_0}{k_{\text{B}}T} + \ln\left(\frac{1-x}{x}\right) + bx + cx^2 + dx^3 \quad (7)$$

where $\Delta\mu_0$ is the standard chemical potential difference, and $x = x_{\text{Rh}}$. By integrating equation (7) with respect to composition we obtain the variation of the free energy with x at each temperature. The value of $\Delta\mu_0$ obtained in the fitting is almost independent of the temperature, varying from $168.0 \text{ kJ mol}^{-1}$ at 900 K to $165.5 \text{ kJ mol}^{-1}$ at 1400 K. Values of $\Delta\mu_0/k_{\text{B}}T$, b , c and d at 900, 1200 and 1400 K are collected together in table 2.

In figure 6 we plot the calculated values of ΔG_{mix} vs x_{Rh} at 900 K, 1200 K and 1400 K, respectively. This figure confirms that at 900 K, one- and two-phase regions are formed at different compositions, and hence it corresponds to a temperature below the consolute temperature, and the negative values of ΔG_{mix} over all compositions at 1400 K are consistent with complete miscibility. Given curves such as those in figure 6, a straightforward common tangent construction at each temperature yields the phase diagram given in figure 7. Overall, the agreement with experiment is satisfactory given the relative crudity of the potential model. The calculated phase diagram lies between those determined experimentally [6, 7, 22, 23], which are also shown in figure 7. The region near $x_{\text{Rh}} = 0.5$ is rather flat, in apparent agreement with the experimental data. The calculated phase diagram is symmetric about $x_{\text{Rh}} = 0.5$ with consolute temperature $\approx 1300 \text{ K}$. We do not see the small asymmetry seen in [6, 22]. Note

Table 2. Values of $\Delta\mu_0/k_{\text{B}}T$, b , c and d (all dimensionless), as defined in equation (7), at $T = 900$, 1200 and 1400 K, obtained by fitting values of $\Delta\mu/k_{\text{B}}T$ calculated at a number of compositions.

T (K)	$\Delta\mu_0/k_{\text{B}}T$	b	c	d
900	22.451	-12.955	15.922	-10.651
1200	16.708	-8.089	7.697	-5.151
1400	14.222	-6.227	4.968	-3.324

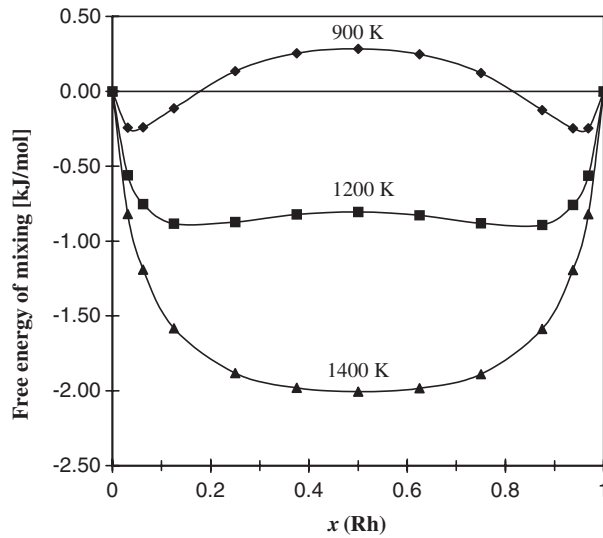


Figure 6. Variation of ΔG_{mix} vs $x(\text{Rh})$, calculated at 900, 1200 and 1400 K.

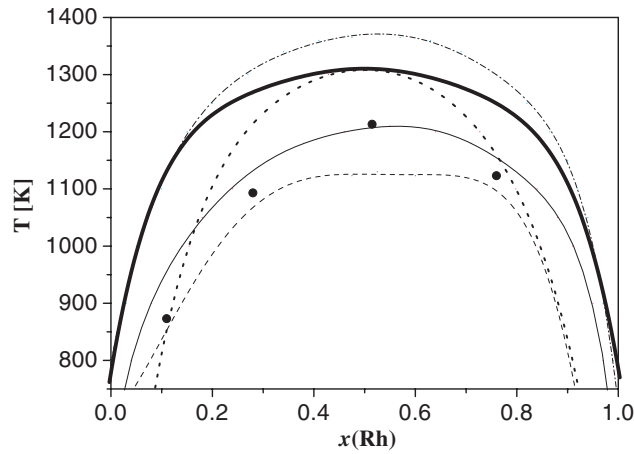


Figure 7. Calculated and experimental phase diagram for Rh/Pd. Our calculations: — (binodal) and ····· (spinodal). Experiment: Shield and Williams [6] (●), Elliot [22] (- - -), Jacob *et al* [7] (—) and diagram obtained in [7] from the thermodynamic data of Myles [23] (- · -).

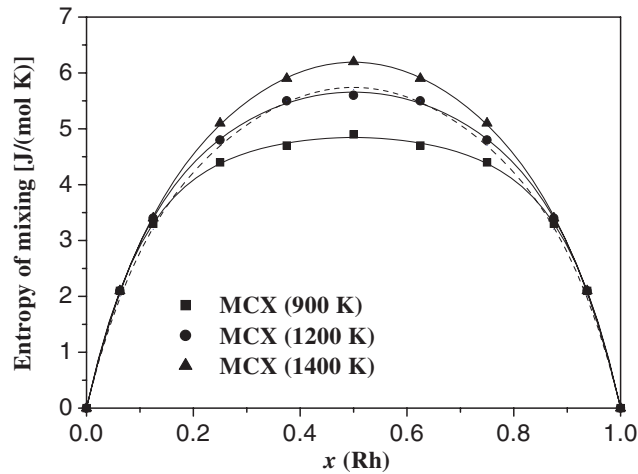


Figure 8. Calculated entropies of mixing at 900, 1200 and 1400 K. The ideal entropy of mixing (ΔS_{ideal}) is also shown (- - -).

that no constraints on the symmetry of the phase diagram are imposed in the calculations. See [4, 13] for calculations on ceramic systems with asymmetric phase diagrams which are reproduced using this approach.

A further advantage of using the semigrand-canonical ensemble is that it is also straightforward to extract the spinodal, which defines the region where a single phase is kinetically as well as thermodynamically unstable with respect to the formation of two separate phases, from the positions of the maxima and minima in the $\Delta\mu_{\text{Mg/Mn}}$ curves in figure 5. The calculated spinodal is also plotted in figure 7.

Finally, we determine entropies of mixing, ΔS_{mix} , from our calculated values of ΔH_{mix} and ΔG_{mix} . Figure 8 shows the resulting variation of ΔS_{mix} with composition at 900, 1200 and 1400 K. For comparison, the ideal entropy of mixing (ΔS_{ideal}) is also plotted. ΔS_{mix} , like

ΔH_{mix} , increases markedly with temperature. At 900 K, ΔS_{mix} is less than the ideal value. At 1200 K, it is close to ideal and is larger than ideal at 1400 K. In this context, it is crucial to realize that the calculated ΔS_{mix} includes *both* configurational *and* vibrational terms, which are often neglected. Our calculated entropy of mixing is appreciably smaller than that in [6], by over $1.5 \text{ J mol}^{-1} \text{ K}^{-1}$ for the 50/50 mixture.

4. Conclusion

In this paper we have used *ab initio* density functional calculations to obtain a potential for Pd–Rh mixtures and used semigrand-canonical ensemble simulations with these new potentials to obtain the phase diagram which is in very good agreement with experiment. The key feature of our Monte Carlo methods, which is applicable to any composition, is that it samples many configurations, explicitly considering different arrangements of atoms, and allows for the *local* structural relaxation surrounding each atom. This relaxation is crucial. If ignored, the energy of exchange of two atoms is usually high and all exchanges are rejected, thus sampling only one arrangement. Vibrational effects are included and the method can be used at any pressure and temperature. Work is currently in progress to develop the methods further and to apply them to more complex systems.

Acknowledgments

This work was funded by EPSRC grants GR/M34799, GR/M53899 and ANPCyT grant BID 802/OC-AR-PICT0361. GDB acknowledges support from el Consejo Nacional de Investigaciones Científicas y Técnicas de la República Argentina, and his contribution to this work has been possible due to a grant from the Fundación Antorchas.

References

- [1] Ducastelle F 1991 *Order and Phase Stability in Alloys* (New York: North-Holland)
- [2] Stocks G M, Nicholson D M C, Shelton W A, Gyorffy B L, Pinski F J, Johnson D D, Staunton J B, Ginatempo B, Turchi P E A and Sluiter M 1991 *Statics and Dynamics of Alloy Phase Transformations* ed P E A Turchi and A Gonis (New York: Plenum) p 305
- [3] Zunger A 1994 *Statics and Dynamics of Alloy Phase Transformations* ed P E A Turchi and A Gonis (New York: Plenum) p 361
- [4] de Fontaine D 1994 *Solid State Physics* vol 47, ed H Ehrenreich and D Turnbull (New York: Academic) p 33
- [5] Ceder G, Van der Ven A, Marianetti C and Morgan D 2000 *Modelling Simul. Mater. Sci. Eng.* **8** 311
- [6] Barrera G D, de Tandler R H and Isoardi E P 2000 *Modelling Simul. Mater. Sci. Eng.* **8** 389
- [7] Allan N L, Barrera G D, Fracchia R M, Lavrentiev M Yu, Taylor M B, Todorov I T and Purton J A 2001 *Phys. Rev. B* **63** 094203
- [8] Lavrentiev M Yu, Allan N L, Barrera G D and Purton J A 2001 *J. Phys. Chem. B* **105** 3594
- [9] Massalski T B (ed) 1986 *Binary Alloy Phase Diagrams* (Metals Park, Ohio: American Society for Metals)
- [10] Shield J E and Williams R K 1987 *Scr. Met. Mat.* **21** 1475
- [11] Jacob K T, Priya S and Waseda Y 1998 *J. Phase Equilib.* **19** 340
- [12] Daw M S and Baskes M I 1984 *Phys. Rev. B* **29** 6443
- [13] Finnis M W and Sinclair J E 1984 *Phil. Mag. A* **50** 45
- [14] Ercolessi F, Parrinello M and Tosatti E 1988 *Phil. Mag.* **58** 213
- [15] Ercolessi F and Adams J B 1994 *Europhys. Lett.* **26** 583
- [16] Purton J A, Barrera G D, Allan N L and Blundy J D 1998 *J. Phys. Chem. B* **102** 5202
- [17] Allan N L, Barrera G D, Lavrentiev M Yu, Todorov I T and Purton J A 2001 *J. Mater. Chem.* **11** 63
- [18] Metropolis N I, Rosenbluth A W, Rosenbluth M N, Teller A N and Teller E 1953 *J. Chem. Phys.* **21** 1087
- [19] Frenkel D and Smit B 2002 *Understanding Molecular Simulation* 2nd edition (San Diego: Academic)
- [20] Perdew J P, Burke S and Ernzerhof M 1996 *Phys. Rev. Lett.* **77** 3865

-
- [17] Blaha P, Schwarz K and Luitz J (ed) 1997 *WIEN97, A Full Potential Linearized Augmented Plane Wave Package for Calculating Crystal Properties* (Vienna: Austria)
 - [18] Kohn W and Sham L J 1965 *Phys. Rev.* **140** A1133
 - [19] Kofke D A and Glandt E D 1988 *Mol. Phys.* **64** 1105
 - [20] Laradji M, Landau D P and Dünweg B 1995 *Phys. Rev. B* **51** 4894
 - [21] Raub E, Beeskow H and Menzel D 1959 *Z. Metallkd.* **50** 428
 - [22] Elliot R P 1965 *Constitution of Binary Alloys, First Supplement* (New York: McGraw-Hill)
 - [23] Myles K M 1968 *Trans. Met. Soc. AIME* **242** 1523